HHS Public Access

Author manuscript

Biomed Mater. Author manuscript; available in PMC 2019 March 16.

Published in final edited form as:

Biomed Mater. ; 13(3): 034108. doi:10.1088/1748-605X/aaad77.

Effects of Tissue Processing on Bioactivity of Cartilage Matrix-Based Hydrogels Encapsulating Osteoconductive Particles

Jakob M. Townsend[1], **Taylor A. Zabel**[2], **Yi Feng**[3], **Jinxi Wang**[3], **Brian T. Andrews**[4], **Randolph J. Nudo**[5], **Cory J. Berkland**[6], and **Michael S. Detamore**[1]

[1]Stephenson School of Biomedical Engineering, University of Oklahoma, Norman, OK 73019

[2]Department of Molecular Biosciences, University of Kansas, Lawrence, KS 66047

[3]Department of Orthopedic Surgery, University of Kansas Medical Center, Kansas City, KS 66160

[4]Department of Plastic Surgery, University of Kansas Medical Center, Kansas City, KS 66160

[5]Department of Rehabilitation Medicine, University of Kansas Medical Center, Kansas City, KS 66160

[6]Department of Pharmaceutical Chemistry, University of Kansas, Lawrence, KS 66047

Abstract

In the treatment of severe traumatic brain injury (TBI), decompressive craniectomy is commonly used to remove a large portion of calvarial bone to allow unimpeded brain swelling. Hydrogels have the potential to revolutionize TBI treatment by permitting a single-surgical intervention, remaining pliable during brain swelling, and tuned to regenerate bone after swelling has subsided. With this motivation, our goal is to present a pliable material capable of regenerating calvarial bone across a critical size defect. We therefore proposed the use of a methacrylated solubilized decellularized cartilage (MeSDCC) hydrogel encapsulating synthetic osteogenic particles of hydroxyapatite nanofibers (HAPnf), bioglass microparticles (BG), or added rat bone marrow-derived mesenchymal stem cells (rMSCs) for bone regeneration in critical-size rat calvarial defects. Fibrin hydrogels were employed as a control material for the study. MeSDCC hydrogels exhibited sufficient rheological performance for material placement before crosslinking (τ_y > 500 Pa), and sufficient compressive moduli post-crosslinking (E > 150 kPa). *In vitro* experiments suggested increased calcium deposition for cells seeded on the MeSDCC material; however, *in vivo* bone regeneration was minimal in both MeSDCC and fibrin groups, even with colloidal materials or added rMSCs. Minimal bone regeneration in the MeSDCC test groups may potentially be attributed to cartilage solubilization after decellularization, in which material signals may have degraded from enzymatic treatment. Looking to the future, an improvement in the bioactivity of the material will be crucial to the success of bone regeneration strategies for TBI treatment.

1. Introduction

Traumatic brain injury (TBI) is characterized by severe brain swelling commonly resulting from motor vehicle accidents, assaults, and stroke. Active duty military service members are especially vulnerable to this condition, as an estimated 22% of wounded soldiers evacuated

from conflict zones have severe TBI.(1) The brain swelling that results from TBI can be life-threatening as the brain lies within a closed cranial vault incapable of expansion to mitigate rising intracranial pressures. Currently, severe TBI is treated by a two-stage surgical intervention. In the first stage, a large portion of calvarial bone is removed in a procedure termed decompressive craniectomy.(2) Decompressive craniectomy allows the brain to swell beyond the cranial vault and reduces dangerous intracranial pressure.(3) After brain swelling has sufficiently decreased, typically weeks to months later, a second procedure termed cranioplasty is performed to restore the skull anatomy and reclose the cranial vault.(4) Disadvantages of the current two-stage TBI surgical intervention are that it prolongs neurorehabilitation and recovery, increases medical costs, and is associated with adverse neurologic symptoms termed syndrome of the trephined.(5) Syndrome of the trephined, also known as sinking skin flap syndrome, is manifested by symptoms such as headaches, unsteadiness, a feeling of apprehension, difficulties concentrating, and fine-motor dexterity concerns. Interestingly, these often debilitating neurologic symptoms of syndrome of the trephined are immediately reversible with a cranioplasty procedure to restore the cranial vault anatomy.(6, 7) Previous attempts to combine the two-stage TBI treatment into a single surgery have resulted in extremely high complication rates due to the inability of materials to expand as initial brain swelling occurs.(8) Current commercial bone products for cranioplasty have been unsuccessful in meeting the demand required for TBI treatment, in either single or two-stage surgical approaches.

Current materials used in commercially available cranioplasty products for bone repair include allogenic bone, synthetic calcium-apatite, and custom polymer/metallic implants.(9) Products that utilize allogenic bone, such as DBX® (MTF/Synthes) and AlloFuse® (AlloSource), have reported advantages of favorable material integration and low rejection; however, issues with batch variability have been noted as potential limitations of using human bone matrix.(10, 11) Current allogenic bone products have limited use in cranioplasty procedures with large cranial defects, termed critical size defects, resulting in reasonable bone regeneration at the defect periphery but minimal regeneration centrally. Synthetic calcium-apatite products, such as NovaBone Putty® (NovaBone Products), which utilize synthetic processes for high-reproducibility, are reported to have acceptable osteoconductive material properties.(12) Similar issues using synthetic apatite approaches compared to allogenic bone products persist with regard to limited bone regeneration across large defect sizes. Cranioplasty approaches utilizing custom-made implants generated based on computed-tomography have gained popularity within the medical community for their patient-specificity.(9, 13) Although custom-made implants are attractive for repairing the cranial vault, they lack in their ability to regenerate calvarial bone, and cannot be implemented in a single surgery for TBI cases due to issues with material flexibility during brain swelling. Beyond commercial products, research avenues for TBI-related issues have generally focused on easing transition between decompressive craniectomy and cranioplasty,(4) or focused on intracerebral regenerative medicine.(14–18) Major gaps in current knowledge exist regarding materials capable of regenerating bone in critical size defects, and in materials that can be implemented in a single surgery for treatment of TBI while avoiding syndrome of the trephined. The first step in meeting the overall goal of developing a single surgical intervention for the treatment of TBI is to first identify a pliable material capable of

regenerating calvarial bone across a critical size defect. Once the first step has been achieved, the regenerative medicine community can focus on translating materials for treatment of TBI. Hydrogels are a promising class of materials for calvarial bone regeneration and future TBI application, offering the capability for *in situ* placement, allowing for application to any shape or size of defect, photocrosslinking for user-defined material activation, and modulation of stiffness for material elasticity during brain swelling.(19)

The objective of the current study was to evaluate the use of a methacrylated solubilized decellularized cartilage (MeSDCC) hydrogel encapsulating synthetic osteogenic particles of hydroxyapatite nanofibers (HAPnf), bioglass microparticles (BG), or added rat bone marrow-derived mesenchymal stem cells (rMSCs) for bone regeneration in critical size rat calvarial defects. Fibrin hydrogels were used as a control material for the study. Fibrin glue was approved by the FDA in 1998 and has been previously used in dental and craniofacial clinical applications.(20–23) The combinational use of photo-crosslinking cartilage-based hydrogel matrix in combination with synthetic particles represents a next-generation approach from our previously published work in the area.(24) The choice of cartilage as a material to facilitate bone regeneration is inspired by the process of endochondral ossification during fracture healing. In a previous publication from our group, the three phases of endochondral ossification: inflammatory, reparative, and remodeling, were reviewed in detail.(25) During the reparative phase, a fibrous and cartilaginous tissue forms spanning the defect. The use of cartilage in the current study attempted to circumvent the initial phases of the endochondral ossification process to accelerate the formation of bone by delivering a similar tissue. Although the calvarium forms from intramembranous ossification, endochondral ossification can be leveraged as an attractive route to increase bone regeneration. Previous *in vitro* studies conducted by our group using rMSCs encapsulated in cartilage-based hydrogels demonstrated an initial increase of collagen I gene expression.(26) The combination of *in vitro* data regarding cartilage-based hydrogels and *in vivo* results using cartilage as a biomaterial for bone regeneration inspired further evaluation of cartilage in calvarial bone regeneration. The addition of synthetic particles to the hydrogel matrix serves a dual purpose, to create a paste-like consistency to facilitate material placement by the surgeon, and to aid in bone regeneration by delivering osteogenic materials. We hypothesized that decellularized cartilage-based hydrogel would facilitate bone regeneration, and that the addition of synthetic osteogenic particles would further improve overall bone regeneration.

2. Materials and Methods

Preparation of Decellularized Cartilage (DCC)

Ten porcine knees were purchased from a local abattoir (Bichelmeyer Meats, Kansas City, KS). Hyaline cartilage was harvested from castrated male Berkshire hogs, 7–8 months of age and 120 kg in weight. The cartilage processing and decellularization protocol is described in our previous publication.(27) Briefly, harvested hyaline cartilage was rinsed, strained, then coarse-ground using a cryogenic tissue grinder (BioSpec Products, Bartlesville, OK). The coarse-ground cartilage was then packed into dialysis tubing (MWCO

3500) packets. Decellularization was achieved through a series of solution exchanges of osmotic shock, detergent, and enzymatic washes as described in our previously established protocols.(28–30) Dialysis packets containing cryoground cartilage were placed in hypertonic salt solution (HSS) at room temperature under agitation (70 rpm) overnight. Dialysis packets were then washed in triton X-100 (0.01 v/v) at 220 rpm, followed by HSS, with DI washes between each step to permeabilize cellular membranes. Dialysis packets were then treated with benzonase enzyme solution (0.0625 KU/mL) at 37°C overnight followed by DI washing before treatment with sodium-lauroylsarcosine (NLS, 1% v/v) overnight for cell lysis and protein denaturation. Afterwards, dialysis packets were washed with DI water then 40% (v/v) ethanol at 70 rpm. Dialysis packets were then soaked in DI water with organic exchange resins to remove organic material from solution. Dialysis packets were then subjected to a saline-mannitol solution followed by DI washes. The tissue was then removed from the tissue packets, frozen, and lyophilized. After decellularization, DCC particles were cryoground using a freezer-mill (SPEX 6775, SamplePrep, Metuchen, NJ). Cryoground DCC was stored at −20°C for later use. The decellularization process was confirmed by the Quant-iT™ PicoGreen™ assay (Cat# P7589, Thermo Fisher Scientific, Waltham, MA).

Synthesis of Methacrylated Solubilized Decellularized Cartilage (MeSDCC)

Solubilization and methacrylation of DCC was achieved using a protocol from our previously reported methods.(31) Briefly, solubilized DCC (sDCC) was created by mixing DCC powder in 0.1 M HCL at a concentration of 10 g/L. Pepsin (Cat# P7000, Sigma-Aldrich, St. Louis, MO) was then added to the DCC-HCL solution at a concentration of 1 g/L and stirred at 200 rpm for 48 hours at room temperature. The solution was then brought to physiological pH by adding 1 M NaOH. The solubilized DCC was then centrifuged at 7,000 × g for 5 min to pellet any unsolubilized DCC particles. The supernatant was then retained, frozen, and lyophilized for later use as sDCC.

MeSDCC was synthesized by first dissolving sDCC in a 1:1 water:acetone mixture at a concentration of 10 g/L. sDCC was then reacted with 20-fold molar excess of glycidyl methacrylate (Cat# 779342, Sigma-Aldrich) in the presence of triethylamine (Cat# T0886, Sigma-Aldrich) and tetrabutylammonium bromide (Cat# 426288, Sigma-Aldrich). The reaction was then stirred at 200 rpm for 6 days at room temperature. Afterward, MeSDCC was precipitated in an excess of acetone, then centrifuged at 3,000 × g for 3 min to pellet the MeSDCC. Pelleted MeSDCC was then dialyzed in DI water for 48 hours before freezing and lyophilizing for later use. The molar excess of glycidyl methacrylate to sDCC was approximated based on reacting one glycidyl methacrylate group to every monomer present in solution, assuming all monomers present were hyaluronic acid.

Rat Bone Marrow Harvest and Culture

rMSCs were harvested from the femurs of a male Sprague-Dawley rat (200–250 g) following an approved IACUC protocol at the University of Kansas (AUS #175-08). The rMSCs were cultured for 1 week in minimum essential medium-α (MEM-α, Cat# 12561072, Thermo Fisher Scientific, Waltham, MA) with 10% fetal bovine serum (FBS, Cat# 16000044, Thermo Fisher Scientific) and 1% antibiotic-antimyotic (anti-anti, Cat#

15240-062, Thermo Fisher Scientific) to ensure no contamination after harvest. After 1 week of culture, the antibiotic-antimyotic was substituted for 1% penicillin/streptomycin (Cat# 15140-122, Thermo Fisher Scientific). Medium was exchanged every other day and cells were cultured until passage 3 before encapsulating the cells in material.

Hydrogel Preparation

MeSDCC hydrogels were prepared as previously described.(24) Briefly, 100 mg of MeSDCC and 100 mg of particles were weighed dry and combined. Hydroxyapatite nanofibers (HAPnf) were bestowed from Nanova Biomaterials, Inc. (Columbia, MO), and 1393-B3 bioglass (BG) microparticles (D_{avg} = 75 – 125 μm) were gifted from MO-SCI, Corp. (Rolla, MO). 1393-B3 BG is a borate glass containing 53% B_2O_3 (wt/wt). Dry material combinations were sterilized using ethylene oxide gas (AN74i, Anderson Anprolene, Haw River, NC) prior to use *in vivo*. Dry combinations were dispersed in 1 mL of phosphate buffered saline (PBS, Cat# P3813, Sigma-Aldrich) solution containing 0.05% 2-Hydroxy-4′-(2-hydroxyethoxy)-2-methylpropiophenone (I2959, Cat# 410896, Sigma-Aldrich) as the photo-initiator. The MeSDCC group with added rMSCs was made by making a 2× concentration of MeSDCC in PBS containing 0.1% I2959, and an equal volume of medium with cells was added to the 2× material and mixed, bringing the final rMSC concentration to 10^6 cells/mL. MeSDCC groups were loaded into 1 mL sterile syringes for later use.

Fibrin hydrogels were created using a dual syringe (2×2 mL, 1:1 ratio) and mixing tip (3×6 mm) purchased from Merlin Packaging Technologies (Gahanna, OH). Due to the quick setting time of enzymatically crosslinked fibrin hydrogels, the dual syringe system was necessary to stop the material from prematurely crosslinking. In the first compartment, Human fibrinogen 1 (Cat# Fib1, Enzyme Research Labs, South Bend, IN) was dissolved in pooled normal plasma (Cat# 0010-5, George King Biomedical, Overland Park, KS) at a concentration of 10% (w/v). The second compartment contained a solution of 20 units/mL of human α-thrombin (Cat# HT1002A, Enzyme Research Labs) dissolved in a 40 mM $CaCl_2$ solution. After mixing, the final concentration was 5% fibrinogen, 10 units/mL of human α-thrombin, 20 mM $CaCl_2$, dissolved in a 50% (v/v) solution of normal human plasma. Fibrin groups with particles (HAPnf or BG) were added equally to both syringes of the dual mixing syringe at a concentration of 10% (w/v). The fibrin group with cells was achieved by mixing concentrated cells and medium with 20 units/mL human α-thrombin and 40 mM $CaCl_2$ in the dual syringe. The final concentration of components was the same as the other groups, with a final cell concentration of 10^6 cells/mL.

Rheological Testing of Hydrogel Precursor Solution

Hydrogel precursor solution yield stress was determined using an AR2000 controlled stress rheometer (TA-Instruments, New Castle, DE). Measurements were performed using a gap distance of 500 μm using a 20-mm diameter crosshatched stainless steel plate geometry and a crosshatched Peltier plate cover at 37°C (n = 5). Precursor yield stress was measured over an oscillatory shear stress sweep from 1–3000 Pa. The yield stress of each material was determined by the cross-over point of the storage (G′) and loss modulus (G″). Hydrogel

precursor solutions were prepared as previously described, with the exception that the fibrin groups were prepared without the enzymatic crosslinker α-thrombin.

Mechanical Testing of Crosslinked Hydrogel

The crosslinked hydrogel compressive modulus (n = 5) was determined using an RSA III dynamic mechanical analyzer (TA-Instruments). Hydrogels for mechanical testing were prepared as previously described.(32) Briefly, hydrogel precursor solution was loaded into a 2 mm thick Teflon mold sandwiched between glass microscope slides. MeSDCC hydrogels were crosslinked with a 312 nm UV-light at 9 mW/cm^2 for 10 min (EB-160C, Spectroline, Westbury, NY). Fibrin hydrogels were crosslinked by injecting the two precursor solutions into the mold space using the dual syringe with mixing tip, the fibrin mixture was allowed to set for 5 min. After crosslinking, circular hydrogels were cut using a sterile 3 mm biopsy punch. hydrogels were pre-swollen in PBS for 24 hours before mechanical testing. The swollen hydrogel diameter was measured using a stereo microscope (20× magnification) and a micrometer, and the hydrogel height was measured using the RSA III. Hydrogels were compressed at a constant rate of 0.005 mm/s until mechanical failure.(33) The compressive modulus was calculated from the slope of the linear portion of the stress-strain curve between 10–20% strain.

In Vitro Cell Study

In vitro studies evaluated the MeSDCC material using the aforementioned media (MEM-α + FBS + anti-anti) supplemented with 10 mM β-glycerophosphate (Cat# G9422, Sigma-Aldrich), 100 nM dexamethasone (Cat# D4902, Sigma-Aldrich), and 250 μM L-ascorbic acid (Cat# A4544, Sigma-Aldrich). MeSDCC material was prepared as previously described and approximately 50 μL of material was injected into the well of a 96-well plate and crosslinked using a handheld 312 nm UV-light. rMSCs were seeded at a concentration of 66,666 cells/mL (150 μL, 10,000 cells/well) on MeSDCC hydrogel or tissue culture treated plastic (n=5). At time points of 2 and 14 days, cells were lysed using 200 μL of cell lysis buffer (Cat# R1060-1-50, Zymo Research, Irvine, CA). DNA content was assayed using the Quant-iT™ PicoGreen™ assay according to the manufacturer's protocol (n = 5). Calcium content was assayed using the QuantiChrom™ calcium assay kit (Cat# DICA-500, BioAssay Systems, Hayward, CA) according to the manufacturer's protocol (n = 5).

Animal Model and Surgical Method

Animal experiments were approved by the Institutional Animal Care and Use Committee of the University of Kansas Medical Center (protocol #2015-2303). The animal model and surgical method was conducted as previously described.(24) Briefly, mixed-sex Sprague-Dawley rats were raised to an age of 7–10 weeks in-house and randomly assigned to treatment groups (n = 5). An incision was created on the posterior periphery of the skull to pull back the skin and periosteum exposing the calvarium. A critical-size (7.5 mm diameter) full thickness bone defect was created in the center of the calvarium (parietal bone) using a dental trephine. The circular piece of calvarial bone was removed, leaving the dura mater intact, and approximately 50 μL of material was syringed into the defect. MeSDCC groups were then crosslinked using a handheld 312 nm UV-light, and fibrin groups were allowed to enzymatically crosslink for 5 min after injection of material. The skin flap was then draped

over the defect site and sutured to hold the material in place during the recovery period. The sham group, which has been republished from our previous study, received the same surgical method without the addition of material.(24) The DBX® group received approximately 50 μL of DBX® Putty. The treated and untreated calvarial bone defects were harvested with the surrounding bone at 8 weeks post-implantation.

Micro-computed Tomography (μCT)

Micro-computed tomography was performed on harvested rat calvarial bone after the 8-week recovery period to quantify new bone. A MicroXCT-400 (Carl Zeiss X-ray Microscopy, Pleasanton, CA) system with a 50-kV X-ray source at 7.9 W was used and a voxel resolution of 39 μm was achieved using the macro-lens. Reconstructed μCT scans were analyzed using Avizo Fire computational software (FEI Company, Hillsboro, OR) to quantify bone formation. Bone was quantified within a cylindrical volume of interest (VOI) of 7.5 mm in diameter and 2 mm in height and centered over the original defect site. The VOI was chosen as the diameter matched the original calvarial defect diameter. Uninjured calvarial bone was used to define the minimum global threshold limit of 35,000. The global threshold was used for identifying bone within the VOI. Bone within the original 7.5 mm diameter defect was colored orange to indicate new bone formation. Quantified new bone is presented as the total (mm^3) within the 7.5 mm diameter defect.

Histology and Immunohistochemistry (IHC)

Explanted calvarial bone defect samples were fixed in 10% phosphate-buffered formalin for 48 hours then stored long term in 70% ethanol. Calvarial tissue samples were then decalcified in Calrite media (Cat# 22-046-339, Thermo Fisher Scientific) for 3 weeks before dehydrating in a grade series of ethanol to xylene, then to paraffin wax for embedding. Using a microtome (HM 355S, Thermo Fisher Scientific), 5 μm thick sections were taken and affixed to microscope slides. Tissue slides were heated to 60°C for 20 min to improve adhesion of tissue to slides, then stored long term at −20°C. Before staining, tissue slides were dewaxed in xylene then rehydrated in a graded series of ethanol (i.e., 100% to 70%) followed by PBS. Slides were stained with hematoxylin and eosin (H&E, Cat# H-3404, Abcam, Cambridge, UK) to visualize cell infiltration and new bone formation.

Immunohistochemistry (IHC) was used to visualize the deposition of collagen I (Cat# NB600-408, Novus Biologicals, Littleton, CO) and collagen II (Cat# NBP2-33343, Novus Biologicals) within the defect site. An in-depth protocol of the IHC procedure has been previously published.(24) Briefly, after tissue dewaxing and rehydrating to PBS with Tween-20 (Cat# P3563, Sigma-Aldrich), antigen retrieval was performed using 20 μg/mL proteinase K (Cat# ab64220, Abcam) for 15 min at 37°C, then cooled at room temperature for 10 min. Sections were then blocked with 0.3% hydrogen peroxide (Cat# ab94666, Abcam) for 10 min, 10% normal horse serum (Cat# PK-6200, Vector Labs, Burlingame, CA) for 20 min, 5% bovine serum albumin (Cat# A9647, Sigma-Aldrich) for 20 min, and avidin/biotin blocking (Cat# SP-2001, Vector Labs) for 15 min each. Sections were then incubated with either 10 μg/mL of collagen I or 5 μg/mL of collagen II (100 μL volume) for 1 hour. After incubation of sections with the primary antibody, slides were washed between each following step using PBS with Tween-20 for 5 min. Sections were then incubated with

biotinylated horse anti-mouse/rabbit IgG (Cat# PK-6200, Vector Labs) for 30 min, VECTASTAIN Elite ABC solution (Cat# PK-6200, Vector Labs) for 30 min, DAB solution (Cat# SK-4100, Vector Labs) for 2 min, DAB-enhancing solution (Cat# H-2200, Vector Labs) for 10 s, counterstained using hematoxylin QS (Cat# H-3404, Vector Labs) for 1 min, bluing solution (Cat# 7301, Thermo Fisher Scientific) for 3 min, then dehydrated in a graded series of ethanol (i.e., 70–100%) to xylene before mounting. Negative controls for each IHC batch were included to confirm negligible background staining.

Statistical Methods

Statistical analyses were conducted using the GraphPad Prism (GraphPad Software Inc, La Jolla, CA) statistical software. A one-way analysis of variance with groups of factors was used to analyze groups. Tukey's post-hoc test was used for comparing between groups. rheological testing, mechanical testing, *in vitro* testing, and μCT had n = 5 samples per group, and data are reported as the mean ± standard deviation.

3. Results

Rheological Analysis of Hydrogel Precursor

Representative rheometer traces are provided for each hydrogel precursor solution that exhibited a yield stress (Fig. 1A). Fibrin and fibrin-BG did not create a noticeable yield stress after being mixed. The yield stress of the MeSDCC-HAPnf group (1641 Pa) was 3.3 and 4.4 times greater than those of the MeSDCC and fibrin-HAPnf group, respectively (Fig. 1B, $p < 0.0001$). The yield stress of the MeSDCC-BG group (1456 Pa) was 2.9 and 3.9 times greater than those of the MeSDCC and fibrin-HAPnf group, respectively ($p < 0.0001$). No significant difference was observed between MeSDCC and fibrin-HAPnf, or between MeSDCC-HAPnf and MeSDCC-BG formulations.

Mechanical Analysis of Crosslinked Hydrogel

Representative stress-strain curves are provided for each material formulation post-crosslinking (Fig. 2A–B). The MeSDCC-HAPnf group (711 kPa) had a compressive modulus that was 4, 26.4, 45.7, and 29.4 times greater than the compressive moduli of the MeSDCC, fibrin, fibrin-HAPnf, and fibrin-BG groups, respectively (Fig. 2C, $p < 0.01$). The MeSDCC-BG group (989 kPa) had a compressive modulus 5.5, 36.7, 63.6, and 40.9 times greater than those of the MeSDCC, fibrin, fibrin-HAPnf, and fibrin-BG groups, respectively ($p < 0.01$). No other differences in modulus were statistically significant.

In Vitro Cell Study

DNA content for MeSDCC or the cell group did not significantly change after 14 days of culture (Fig. 3A). The cell group at day 14 (2.1 μg/mL) had 3.9 times greater DNA content compared to the MeSDCC group at the same time point ($p<0.0001$). Calcium content assayed for the cell group at day 2 was unable to detect calcium in the samples; however, a detectable amount was observed in the MeSDCC group (22.7 μg/mL) (Fig. 3B). A significantly greater increase in calcium was observed for the MeSDCC material at day 14 (50.1 μg/mL) compared to MeSDCC at day 2 ($p<0.0005$). No significant differences were observed for calcium content between the cell group and the MeSDCC group. Calcium

normalized to DNA content revealed that the MeSDCC material at day 14 (92.8 μg/μg) had 4.4 and 4.8 times greater normalized calcium content compared to MeSDCC at day 2 and cells at day 14 ($p<0.0001$) (Fig. 3C)

Micro-computed Tomography (μCT) Analysis

Large bone islands were observed in both the sham and DBX group; however, bone islands observed in the sham group were thin and did not significantly contribute to overall total regenerated bone volume (Fig. 4A). Small bone island formation was observed in all samples except the MeSDCC group and groups containing HAPnf. Peripheral bone growth was observed in all samples. The DBX group (8.94 mm^3) had 2.1, 2.7, 2.8, 4.3, 5.5, 3.1, 3.0, 3.1, and 2.6 times greater bone regeneration compared to the sham, fibrin, fibrin+Cells, fibrin-HAPnf, fibrin-BG, MeSDCC, MeSDCC+Cells, MeSDCC-HAPnf, and MeSDCC-BG groups, respectively (Fig. 4B, $p < 0.05$). No significant difference was observed among any other group.

Histological and Immunohistochemistry (IHC) Analysis

Soft tissue formation spanning the defect site was observed in all samples (Fig. 5). Peripheral bone growth was observed in all samples and tended to form toward the dural side of the defect. No differences were noted among the MeSDCC or Fibrin groups with or without the addition of rMSCs. Groups with exogenously added cells did not appear to have a higher number of stained nuclei within the defect. Groups containing HAPnf had leftover material within the defect site after the 8-week recovery period, and in some samples, cells were unable to migrate to the center of the material. Leftover MeSDCC hydrogel was observed in the MeSDCC-BG group based on collagen II deposition. Leftover BG particles were observed in both MeSDCC and Fibrin hydrogels and tended to migrate to the periphery of the defect site in all samples.

Collagen I staining showed substantial deposition throughout the defect site, including the soft tissue portion (Fig. 6). Native peripheral bone was used as the reference for comparison. In groups containing HAPnf, minimal deposition of collagen I was observed toward the center of the defect. Staining for collagen II showed almost no collagen II deposition within the defect site, except for the MeSDCC-BG group, where small tissue pockets positively staining for collagen II deposition were observed.

4. Discussion

The current study was the first to use an *in situ* crosslinking hydrogel comprised of naturally-derived decellularized cartilage-based matrix for calvarial bone regeneration *in vivo*. The use of a cartilage-based hydrogel for bone regeneration follows our previous work using micronized decellularized hyaline-cartilage particles and hydroxyapatite colloidal gels for bone regeneration *in vivo*.(24) In designing hydrogels with potential for TBI treatment in mind, the mechanical performance of the material before and after UV-crosslinking was identified as a crucial aspect for clinical translation.(19) All MeSDCC hydrogels tested exhibited sufficient yield stress ($\tau_y > 500$ Pa) for material placement, and addition of HAPnf or BG particles significantly increased the yield stress of the material to a range of 1400 to

1600 Pa. For context, the yield stress of mayonnaise is approximately 200 Pa, and the yield stress of Play-Doh is approximately 3000 Pa.(34) The potential reason that only the fibrin-HAPnf led to a detectable yield stress may have been that the fibers would conceivably interact more with their surrounding environment than a sphere due to the randomized fiber orientation distribution, and a changing microstructure from fiber-fiber and fiber-medium interactions.(35) Although the calvarium is a non-load bearing bone, sufficient material mechanical performance is necessary to remain in place during healing, and provide a barrier between the brain and scalp. Due to stiffness being an important parameter for material success, the compressive modulus of hydrogels was characterized. After crosslinking of the hydrogel precursor, MeSDCC hydrogels with colloids had considerably higher compressive moduli compared to fibrin groups; however, no significant difference was observed among the MeSDCC group and the fibrin groups. The addition of colloids in fibrin groups did not increase the compressive modulus as observed in the MeSDCC groups. Comparing fibrin and MeSDCC without particles, MeSDCC on average had a higher compressive modulus, potentially due to a greater crosslinking density. The difference in compressive modulus could be in part due to limited initial crosslinking in fibrin groups compared to MeSDCC, and thus the added colloids were not sufficiently encapsulated in the matrix, or that the MeSDCC material interacted with the particles to a greater extent. Additionally, although the compressive modulus of native bone is on the magnitude of GPa, hydrogels do not necessarily need to match the compressive modulus of native bone in the calvarium due to the non-load bearing nature.(36) The elastic nature of a hydrogel would also be beneficial for future TBI application allowing pliability during brain swelling. For these reasons, we have identified a minimum compressive modulus of 100 kPa, similar to human skin tissue to maintain shape while remaining pliable.(37) Although a minimum compressive modulus has been identified for the current study, it is worth noting that for future TBI application a balance between hydrogel stiffness and pliability will need to be identified to engineer the most attractive option to protect the brain after craniectomy while still allowing material pliability during the brain swelling process.

In vitro experiments suggested an increase matrix calcification for the MeSDCC material after 14 days of culture; however, *in vivo* bone tissue formation within the defect for both fibrin and MeSDCC groups was minimal. No difference in bone formation was observed among any fibrin or MeSDCC formulation. The DBX® group was the only group to outperform the sham control in regenerated bone volume, showing increased bone formation spanning into the defect. Sham groups had noticeable bone island formation covering an ample area; however, the bone formed was especially thin and did not contribute significantly to the overall bone volume. Sporadic small bone island formation was observed in all groups, with the exception of the HAPnf-containing groups. H&E staining revealed a large amount of leftover HAPnfs in both fibrin and MeSDCC formulations. The HAPnf appeared to perhaps inhibit cell migration toward the center of the material. Cell migration issues with HAPnf were especially problematic in combination with MeSDCC, potentially due to the high compressive modulus and yield stress of the material during hydrogel degradation for cellular infiltration. Collagen I deposition was homogeneous throughout all samples except the HAPnf containing groups, where there was minimal positive staining for collagen I in the center of the material, most likely due to the lack of cellular infiltration into

the material. The only material to have leftover hydrogel matrix inside the defect after the 8-week period was the MeSDCC-BG group; however, the remaining volume was especially small and not apparent in all samples. Collagen II deposition was not detected in all samples except for the MeSDCC-BG group, in which the leftover MeSDCC hydrogel positively stained for collagen II. One may argue that the incorporation enzymatically degradable sequences or a material porogen may enhance regenerative capabilities by facilitating cellular infiltration and remodeling. However, the observation of remaining MeSDCC in only one group, juxtaposed with the limited capacity of regeneration even with rMSCs present, leads to the conclusion that the inherent material bioactivity is the primary focus for future improvement becomes, with cell infiltration and migration being relegated to a secondary issue.

Although our group was the first to use naturally derived cartilage for calvarial bone regeneration, other groups have studied the use of cartilage matrix (naturally derived or tissue engineered) for bone formation. Cunniffe *et al.*(38) studied the use of chondrogenically-primed rMSCs encapsulated in alginate hydrogels to partially mimic the endochondral ossification healing process in rat critical-size femur and calvarial defects. The rMSC-alginate hydrogels appeared to support bone formation at the hydrogel surface, and comparable bone regeneration to the current study was observed. In another study from that same group, a decellularized tissue engineered cartilage scaffold was studied for use in long bone defect healing.(39) The tissue engineered cartilage scaffold promoted more bone regeneration on average compared to the sham group; however, a considerable amount of deviation was observed within the group. In yet another study from the same group using decellularized growth plate a significant increase in bone regeneration was observed compared to the sham group.(40) The studies by Cunniffe *et al.* illustrated promise for the use of cartilage-derived matrix/cells in promoting bone regeneration by recapitulating part of the endochondral ossification process. In a study using DCC scaffolds to promote endochondral bone formation, collagen I deposition was observed after 22 days of subcutaneous implantation in a rat model.(41) Similarly, in another study, collagen I deposition and mineralization was observed in gelatin methacrylamide hydrogels encapsulating DCC particles after 8 weeks of *in vivo* rat subcutaneous implantation.(42) In a previous study by our group a significant increase in calvarial bone regeneration was observed using DCC combined with hydroxyapatite compared to the sham defect.(24) The aforementioned studies supported the use of DCC as a material for bone regeneration. In comparing the referred studies to the current study, limited bone regeneration with MeSDCC hydrogels in the current study may potentially have been attributed to the processing of DCC. The further processing of DCC to create MeSDCC may potentially have contributed to a lower bioactivity and subsequent lower bone formation. DCC solubilization is speculated to have been the major contributing factor in the reduction of material bioactivity, as potential signals may have been affected by the process. Reduced bioactivity due to tissue decellularization has been previously discussed, in which devitalized cartilage (DVC) had greater bioactivity than DCC potentially due to altering matrix architecture and a reduction of important growth factors from decellularization.(27) DVC is cartilage extracellular matrix that has only undergone physical processing (i.e., granulating) without the additional step of chemical decellularization.(43) In another study from our group evaluating methacrylated

solubilized devitalized cartilage (MeSDVC) loaded with DVC particles, increased gene expression was observed in MeSDVC hydrogels with DVC particles compared to MeSDVC alone.(26) Therefore, both decellularization and solubilization could potentially contribute to lower bioactivity. Future studies using cartilage will focus on minimizing the processing of cartilage to retain material activity, in which the use of DVC may be of interest for enhancing endochondral bone formation. Further research is necessary to fully characterize the use of cartilage in bone regeneration in general, and in calvarial defect regeneration in particular.

5. Conclusion

MeSDCC hydrogels composed entirely of naturally-derived DCC demonstrated desirable handling properties in the pre-crosslinked form, and appropriate mechanical performance post-crosslinking for a cranioplasty application. The addition of synthetic particles (HAPnf or BG) increased the mechanical stiffness of MeSDCC hydrogels several fold, approaching the 1 MPa mark in compressive modulus, which may be desirable in a TBI application. *In vivo* testing in an 8-week rat calvarial defect model demonstrated minimal bone formation in both MeSDCC and fibrin groups containing osteoconductive particles. Encapsulated rMSCs did not appear to influence bone formation in either fibrin or MeSDCC hydrogels, and significant bone formation was only observed in the DBX® group, suggesting that material bioactivity may be the governing limitation beyond cell infiltration. Minimal bone formation using MeSDCC compared to other published studies potentially suggests that DCC solubilization may have potentially reduced material activity in this application. Further research is necessary to determine the full capacity of cartilage (DCC and DVC) as a material to promote bone regeneration.

Acknowledgments

The authors would like to thank Nanova Biomaterials, Inc. and MO-SCI, Corp. for generously providing the hydroxyapatite nanofibers and bioglass microparticles, respectively. We would like to recognize funding from the Kansas Bioscience Authority Rising Star Award and the Stephenson Graduate Fellowship. Research reported in this publication was supported by the National Institute of Dental and Craniofacial Research of the National Institutes of Health under Award Number R01 DE022472. The content is solely the responsibility of the authors and does not necessarily represent the official views of the National Institutes of Health.

References

1. Risdall JE, Menon DK. Traumatic brain injury. Philos Trans R Soc Lond B Biol Sci. 2011; 366(1562):241–50. [PubMed: 21149359]
2. Cushing H. The establishment of cerebral hernia as a decompressive measure for inaccessible brain tumors: with the description of intermuscular methods of making the bone defect in temporal and occipital regions. 1905
3. Yang XF, Wen L, Shen F, Li G, Lou R, Liu WG, et al. Surgical complications secondary to decompressive craniectomy in patients with a head injury: a series of 108 consecutive cases. Acta Neurochir (Wien). 2008; 150(12):1241–7. discussion 8. [PubMed: 19005615]
4. Oladunjoye AO, Schrot RJ, Zwienenberg-Lee M, Muizelaar JP, Shahlaie K. Decompressive craniectomy using gelatin film and future bone flap replacement. J Neurosurg. 2013; 118(4):776–82. [PubMed: 23394343]
5. Grant FC, Norcross NC. Repair of cranial defects by cranioplasty. Annals of surgery. 1939; 110(4): 488. [PubMed: 17857467]

6. Dujovny M, Agner C, Aviles A. Syndrome of the trephined: theory and facts. Crit Rev Neurosurg. 1999; 9(5):271–8. [PubMed: 10525845]
7. Schiffer J, Gur R, Nisim U, Pollak L. Symptomatic patients after craniectomy. Surgical Neurology. 1997; 47(3):231–7. [PubMed: 9068692]
8. Martin KD, Franz B, Kirsch M, Polanski W, von der Hagen M, Schackert G, et al. Autologous bone flap cranioplasty following decompressive craniectomy is combined with a high complication rate in pediatric traumatic brain injury patients. Acta Neurochir (Wien). 2014; 156(4):813–24. [PubMed: 24532225]
9. Khader BA, Towler MR. Materials and techniques used in cranioplasty fixation: A review. Mater Sci Eng C Mater Biol Appl. 2016; 66:315–22. [PubMed: 27207068]
10. Gruskin E, Doll BA, Futrell FW, Schmitz JP, Hollinger JO. Demineralized bone matrix in bone repair: history and use. Adv Drug Deliv Rev. 2012; 64(12):1063–77. [PubMed: 22728914]
11. NaPier Z, Kanim LEA, Thordarson S, Kropf MA, Cuéllar JM, Glaeser JD, et al. Demineralized Bone Matrix Bone Biology and Clinical Use. Seminars in Spine Surgery. 2016; 28(4):196–216.
12. Schallenberger MA, Rossmeier K, Lovick HM, Meyer TR, Aberman HM, Juda GA. Comparison of the osteogenic potential of OsteoSelect demineralized bone matrix putty to NovaBone calcium-phosphosilicate synthetic putty in a cranial defect model. J Craniofac Surg. 2014; 25(2):657–61. [PubMed: 24577306]
13. O'Reilly EB, Barnett S, Madden C, Welch B, Mickey B, Rozen S. Computed-tomography modeled polyether ether ketone (PEEK) implants in revision cranioplasty. J Plast Reconstr Aesthet Surg. 2015; 68(3):329–38. [PubMed: 25541423]
14. Choy DK, Nga VD, Lim J, Lu J, Chou N, Yeo TT, et al. Brain tissue interaction with three-dimensional, honeycomb polycaprolactone-based scaffolds designed for cranial reconstruction following traumatic brain injury. Tissue Eng Part A. 2013; 19(21–22):2382–9. [PubMed: 23691928]
15. Tate M. Biocompatibility of methylcellulose-based constructs designed for intracerebral gelation following experimental traumatic brain injury. Biomaterials. 2001; 22(10):1113–23. [PubMed: 11352091]
16. Tian WM, Hou SP, Ma J, Zhang CL, Xu QY, Lee IS, et al. Hyaluronic acid-poly-D-lysine-based three-dimensional hydrogel for traumatic brain injury. Tissue Eng. 2005; 11(3–4):513–25. [PubMed: 15869430]
17. Wong DY, Hollister SJ, Krebsbach PH, Nosrat C. Poly(epsilon-caprolactone) and poly (L-lactic-co-glycolic acid) degradable polymer sponges attenuate astrocyte response and lesion growth in acute traumatic brain injury. Tissue Eng. 2007; 13(10):2515–23. [PubMed: 17655492]
18. Zhang T, Yan Y, Wang X, Xiong Z, Lin F, Wu R, et al. Three-dimensional Gelatin and Gelatin/Hyaluronan Hydrogel Structures for Traumatic Brain Injury. Journal of Bioactive and Compatible Polymers. 2007; 22(1):19–29.
19. Kretlow JD, Young S, Klouda L, Wong M, Mikos AG. Injectable biomaterials for regenerating complex craniofacial tissues. Adv Mater. 2009; 21(32–33):3368–93. [PubMed: 19750143]
20. Buckley MJ, Beckman EJ. Adhesive use in oral and maxillofacial surgery. Oral Maxillofac Surg Clin North Am. 2010; 22(1):195–9. [PubMed: 20159487]
21. Janmey PA, Winer JP, Weisel JW. Fibrin gels and their clinical and bioengineering applications. J R Soc Interface. 2009; 6(30):1–10. [PubMed: 18801715]
22. Spotnitz WD. Fibrin sealant: past, present, and future: a brief review. World J Surg. 2010; 34(4): 632–4. [PubMed: 19820991]
23. Spotnitz WD. Fibrin Sealant: The Only Approved Hemostat, Sealant, and Adhesive-a Laboratory and Clinical Perspective. ISRN Surg. 2014; 2014:203943. [PubMed: 24729902]
24. Townsend JM, Dennis SC, Whitlow J, Feng Y, Wang J, Andrews B, et al. Colloidal Gels with Extracellular Matrix Particles and Growth Factors for Bone Regeneration in Critical Size Rat Calvarial Defects. The AAPS Journal. 2017; 19(3):703–11. [PubMed: 28138909]
25. Dennis SC, Berkland CJ, Bonewald LF, Detamore MS. Endochondral ossification for enhancing bone regeneration: converging native extracellular matrix biomaterials and developmental engineering in vivo. Tissue Eng Part B Rev. 2015; 21(3):247–66. [PubMed: 25336144]

26. Beck EC, Barragan M, Tadros MH, Kiyotake EA, Acosta FM, Kieweg SL, et al. Chondroinductive Hydrogel Pastes Composed of Naturally Derived Devitalized Cartilage. Ann Biomed Eng. 2016; 44(6):1863–80. [PubMed: 26744243]
27. Beck EC, Barragan M, Libeer TB, Kieweg SL, Converse GL, Hopkins RA, et al. Chondroinduction from Naturally Derived Cartilage Matrix: A Comparison Between Devitalized and Decellularized Cartilage Encapsulated in Hydrogel Pastes. Tissue Eng Part A. 2016; 22(7–8):665–79. [PubMed: 27001140]
28. Sutherland AJ, Beck EC, Dennis SC, Converse GL, Hopkins RA, Berkland CJ, et al. Decellularized cartilage may be a chondroinductive material for osteochondral tissue engineering. PLoS One. 2015; 10(5):e0121966. [PubMed: 25965981]
29. Sutherland AJ, Detamore MS. Bioactive Microsphere-Based Scaffolds Containing Decellularized Cartilage. Macromol Biosci. 2015; 15(7):979–89. [PubMed: 25821206]
30. Converse GL, Armstrong M, Quinn RW, Buse EE, Cromwell ML, Moriarty SJ, et al. Effects of cryopreservation, decellularization and novel extracellular matrix conditioning on the quasi-static and time-dependent properties of the pulmonary valve leaflet. Acta Biomater. 2012; 8(7):2722–9. [PubMed: 22484150]
31. Beck EC, Barragan M, Tadros MH, Gehrke SH, Detamore MS. Approaching the compressive modulus of articular cartilage with a decellularized cartilage-based hydrogel. Acta Biomater. 2016; 38:94–105. [PubMed: 27090590]
32. Beck EC, Lohman BL, Tabakh DB, Kieweg SL, Gehrke SH, Berkland CJ, et al. Enabling Surgical Placement of Hydrogels Through Achieving Paste-Like Rheological Behavior in Hydrogel Precursor Solutions. Ann Biomed Eng. 2015; 43(10):2569–76. [PubMed: 25691398]
33. Rennerfeldt DA, Renth AN, Talata Z, Gehrke SH, Detamore MS. Tuning mechanical performance of poly(ethylene glycol) and agarose interpenetrating network hydrogels for cartilage tissue engineering. Biomaterials. 2013; 34(33):8241–57. [PubMed: 23932504]
34. Samaniuk JR, Shay TW, Root TW, Klingenberg DJ, Scott CT. A novel rheometer design for yield stress fluids. AIChE Journal. 2014; 60(4):1523–8.
35. Eberle APR, Baird DG, Wapperom P. Rheology of Non-Newtonian Fluids Containing Glass Fibers: A Review of Experimental Literature. Industrial & Engineering Chemistry Research. 2008; 47(10):3470–88.
36. Motherway JA, Verschueren P, Van der Perre G, Vander Sloten J, Gilchrist MD. The mechanical properties of cranial bone: the effect of loading rate and cranial sampling position. J Biomech. 2009; 42(13):2129–35. [PubMed: 19640538]
37. Yeung CC, Holmes DF, Thomason HA, Stephenson C, Derby B, Hardman MJ. An ex vivo porcine skin model to evaluate pressure-reducing devices of different mechanical properties used for pressure ulcer prevention. Wound Repair Regen. 2016; 24(6):1089–96. [PubMed: 27717144]
38. Cunniffe GM, Vinardell T, Thompson EM, Daly AC, Matsiko A, O'Brien FJ, et al. Chondrogenically primed mesenchymal stem cell-seeded alginate hydrogels promote early bone formation in critically-sized defects. European Polymer Journal. 2015; 72:464–72.
39. Cunniffe GM, Vinardell T, Murphy JM, Thompson EM, Matsiko A, O'Brien FJ, et al. Porous decellularized tissue engineered hypertrophic cartilage as a scaffold for large bone defect healing. Acta Biomater. 2015; 23:82–90. [PubMed: 26038199]
40. Cunniffe GM, Diaz-Payno PJ, Ramey JS, Mahon OR, Dunne A, Thompson EM, et al. Growth plate extracellular matrix-derived scaffolds for large bone defect healing. Eur Cell Mater. 2017; 33:130–42. [PubMed: 28197989]
41. Gawlitta D, Benders KE, Visser J, van der Sar AS, Kempen DH, Theyse LF, et al. Decellularized cartilage-derived matrix as substrate for endochondral bone regeneration. Tissue Eng Part A. 2015; 21(3–4):694–703. [PubMed: 25316202]
42. Visser J, Gawlitta D, Benders KE, Toma SM, Pouran B, van Weeren PR, et al. Endochondral bone formation in gelatin methacrylamide hydrogel with embedded cartilage-derived matrix particles. Biomaterials. 2015; 37:174–82. [PubMed: 25453948]
43. Sutherland AJ, Converse GL, Hopkins RA, Detamore MS. The bioactivity of cartilage extracellular matrix in articular cartilage regeneration. Adv Healthc Mater. 2015; 4(1):29–39. [PubMed: 25044502]

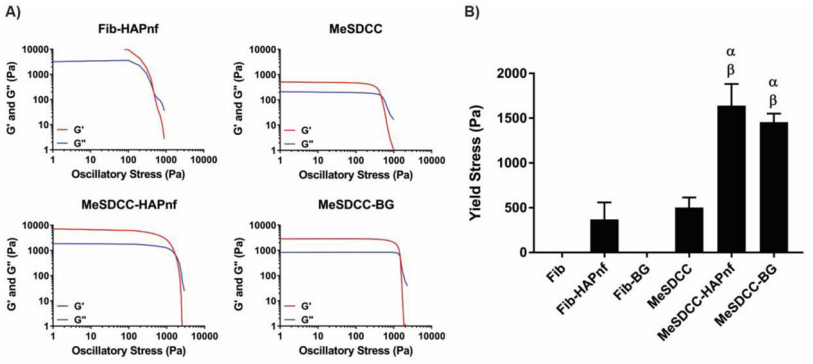

Figure 1.

A) Representative rheometer traces for Fib-HAPnf, MeSDCC, MeSDCC-HAPnf, and MeSDCC-BG hydrogel precursor solutions. B) Hydrogel yield stress determined by the crossover point of the storage (G′) and loss (G″) moduli. α = significant increase compared to MeSDCC ($p<0.0001$) and β = significantly larger value compared to the Fib-HAPnf group ($p<0.0001$). Addition of colloidal particles to MeSDCC significantly increased the yield stress by a factor of ~3. n = 5, values represent the mean ± standard deviation. Fib = Fibrin, MeSDCC = Methacrylated Solubilized Decellularized Cartilage, HAPnf = Hydroxyapatite Nanofibers, BG = Bioglass.

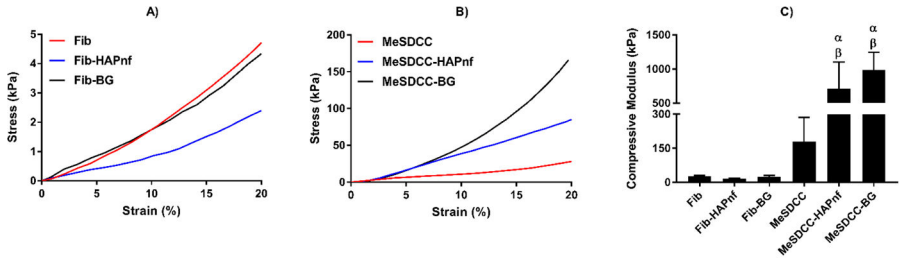

Figure 2.

A–B) Representative stress-strain curves for crosslinked hydrogel groups. C) Compressive modulus determined by the slope of the stress-strain curve between 10 and 20% strain. α = significant increase compared to the MeSDCC group ($p<0.01$) and β = significantly larger than Fib, Fib-HAPnf, and Fib-BG ($p<0.0001$). Addition of colloidal particles to MeSDCC significantly increased the compressive modulus by a factor of 4 to 5.5. n = 5, values represent the mean ± standard deviation. Fib = Fibrin, MeSDCC = Methacrylated Solubilized Decellularized Cartilage, HAPnf = Hydroxyapatite Nanofibers, BG = Bioglass.

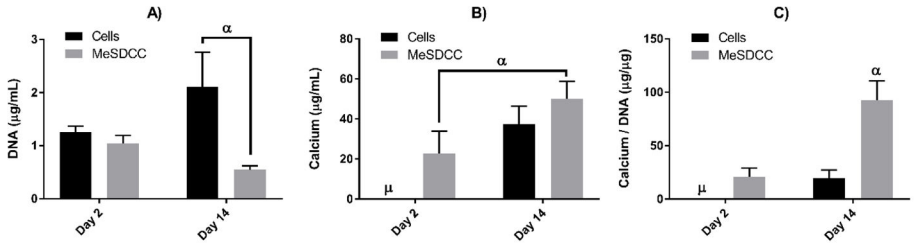

Figure 3.

Biochemical analysis for calcium and DNA content after 14 days of *in vitro* cell culture. A) DNA content after 2 and 14 days. Note significantly different DNA content between the cells seeded on tissue culture treated plastic and MeSDCC. α = Significantly larger value compared to MeSDCC at day 14 ($p<0.0001$). B) Calcium content after 2 and 14 days of cell culture. Note a significant increase in calcium content for the MeSDCC group after 14 days of cell culture. μ = calcium content too low to measure. α = Significantly larger increase compared to MeSDCC at day 2 ($p<0.0005$). C) Total calcium content normalized to intracellular DNA content. Note greater normalized calcium content for the MeSDCC group compared to all other groups. μ = calcium content too low to measure. α = significantly greater normalized calcium content compared to all other groups ($p<0.0001$). n = 5, values represent the mean ± standard deviation. MeSDCC = Methacrylated Solubilized Decellularized Cartilage.

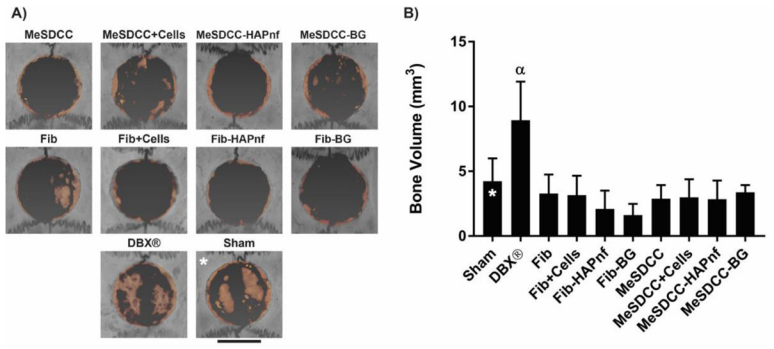

Figure 4.

Microcomputed tomography (μCT) analysis using Avizo software 8 weeks after implantation. A) Reconstructed μCT scans of calvarial defects. Orange coloring indicates regenerated bone to distinguish from existing bone. B) Regenerated bone volume determined by μCT. α = significantly greater bone volume compared to all other groups ($p<0.05$). Note that only the DBX® treatment group had a significantly larger bone volume compared to the sham. Scale bar = 5 mm. Asterisks (*) represent our previously published data (i.e., sham group).(24) n = 5, values represent the mean ± standard deviation. Fib = Fibrin, MeSDCC = Methacrylated Solubilized Decellularized Cartilage, HAPnf = Hydroxyapatite Nanofibers, BG = Bioglass.

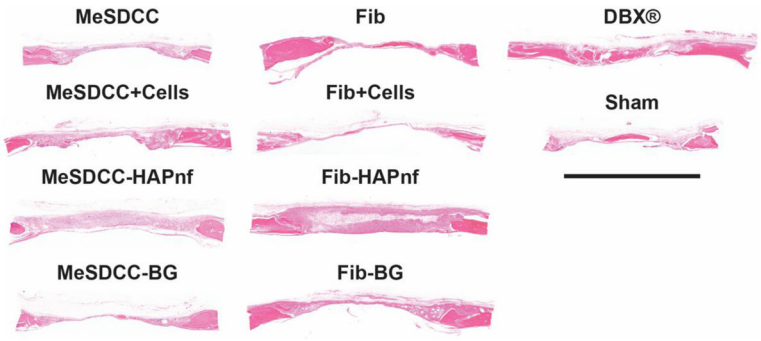

Figure 5.

Hematoxylin and eosin (H&E) histological analysis of critical size (7.5 mm) rat calvarial defects 8 weeks after implantation. Sections were taken in the sagittal plane with the dural side of the calvarium as the bottom of each image. Note that regeneration was limited in all groups except the DBX® group. Scale bar = 5 mm. Fib = Fibrin, MeSDCC = Methacrylated Solubilized Decellularized Cartilage, HAPnf = Hydroxyapatite Nanofibers, BG = Bioglass.

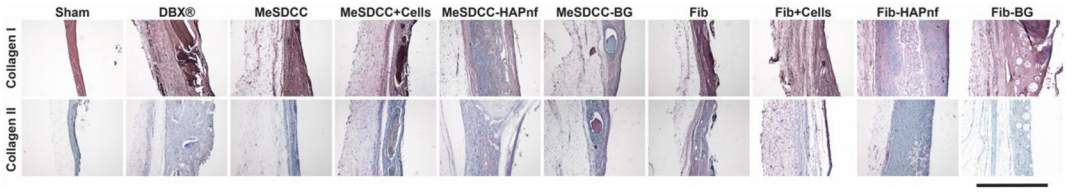

Figure 6.

Immunohistochemical (IHC) staining for collagen I and collagen II. Brown coloring indicates positive presence for the selected antibody, and the blue staining represents the hematoxylin counterstain. Note the positive collagen II staining in the MeSDCC-BG group, indicating leftover hydrogel after the 8-week recovery period. Scale bar = 500 μm. Fib = Fibrin, MeSDCC = Methacrylated Solubilized Decellularized Cartilage, HAPnf = Hydroxyapatite Nanofibers, BG = Bioglass.